Journal of Materials Chemistry A

Accepted Manuscript

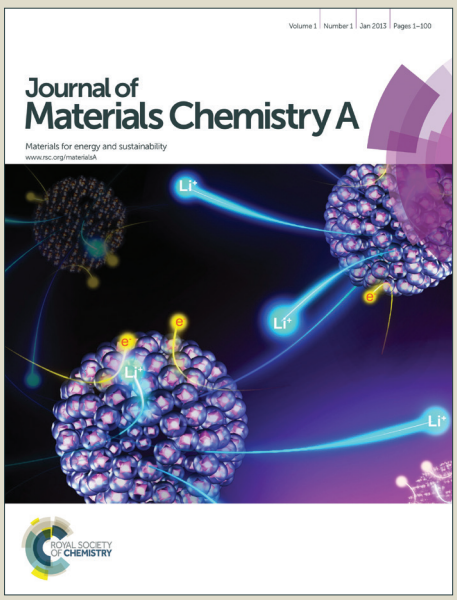

ROYAL SOCIETY OF CHEMISTRY

www.rsc.org/materialsA

PAPER www.rsc.org/materials | Journal of Materials Chemistry A

The effect of oxygen transfer mechanism on the cathode performance based on proton-conducting solid oxide fuel cells

Jie Hou[a], Jing Qian[a], Lei Bi[b,*], Zheng Gong[a], Ranran Peng[a] and Wei Liu[a,c,*]

Received: 26th August 2014

Two kinds of proton-blocking composites $La_2NiO_{4+\delta}$-$LaNi_{0.6}Fe_{0.4}O_{3-\delta}$ (LNO-LNF) and $Sm_{0.2}Ce_{0.8}O_{2-\delta}$-$LaNi_{0.6}Fe_{0.4}O_{3-\delta}$ (SDC-LNF) were evaluated as cathode materials for proton-conducting solid oxide fuel cells (H-SOFCs) based on $BaZr_{0.1}Ce_{0.7}Y_{0.2}O_{3-\delta}$ (BZCY) electrolyte, in order to compare and investigate the influence of two different oxygen transfer mechanism on the performance of the cathode for H-SOFCs. The X-ray diffraction (XRD) results showed that the chemical compatibility of the components in both compounds was excellent up to 1000 °C. Electrochemical studies revealed that LNO-LNF showed lower area specific polarization resistances in symmetrical cells and better electrochemical performance in single cell tests. The single cell with LNO-LNF cathode generated remarkable higher maximum power densities (MPDs) and lower interfacial polarization resistances (R_p) than that with SDC-LNF cathode. Correspondingly, the MPDs of the single cell with LNO-LNF cathode were 490, 364, 266, 180 mW cm^{-2} while the R_p were 0.103, 0.279, 0.587, 1.367 Ω cm^2 at 700, 650, 600 and 550 °C, respectively. Meanwhile, after the single cell with LNO-LNF cathode optimized with an anode functional layer (AFL) between the anode and electrolyte, the power outputs reached 708 mW cm^{-2} at 700 °C. These results demonstrate that LNO-LNF composite cathode with the interstitial oxygen transfer mechanism is a more preferable alternative for H-SOFCs than SDC-LNF composite cathode with the oxygen vacancy transfer mechanism.

1 Introduction

Proton-conducting solid oxide fuel cells (H-SOFCs) have attracted much attention for low-temperature operation because many solid oxide proton conductors display lower activation energy than oxygen-ion conductors such as YSZ and rare-earth doped ceria (DCO), thus having potential for higher proton conductivity and faster surface reactions at lower temperatures.[1-8] In view of its high ionic conductivity, acceptor-doped $BaCeO_3$ is a promising electrolyte candidate for H-SOFCs. Particularly, $BaZr_{0.1}Ce_{0.7}Y_{0.2}O_{3-\delta}$ (BZCY), which has been demonstrated to exhibit not only adequate proton conductivity but also sufficient chemical stability, is one of the most popular proton conductors.[9-11] As an important component of SOFC, cathode must meet certain requirements for proper operation, including adequate electrical conductivity, good catalytic activity, good chemical compatibility and a compatible expansion coefficient (TEC) with the electrolyte.[12] In recent years, many efforts were focused on exploiting high performance cobalt-free cathode materials for H-SOFCs, such as LNO-LNF73[1], BZCY-LNF[12], $La_{0.7}Sr_{0.3}FeO_{3-\delta}$-SDC[9], $Ba_{0.5}Sr_{0.5}Zn_{0.2}Fe_{0.8}O_{3-\delta}$[13], $Ba_{0.5}Sr_{0.5}FeO_{3-\delta}$-SDC[14], $BaCe_{0.5}Bi_{0.5}O_{3-\delta}$[15] and so on.

Up to now, the composite cathode materials developed for H-SOFCs can be mainly divided into two types. One type is the proton-conducting composite cathode (PCCC) that allows simultaneous transport of oxygen vacancies, electronic defects and protons. The other type is the proton-blocking composite cathode (PBCC) which was firstly proposed for H-SOFCs by Sun et al.[9] In the PBCC, dissociated oxygen ions transfer along the surface of the cathode or through the bulk of the cathode to triple phase boundaries (TPBs), and hence the electrochemical reactions mainly occur at the cathode-electrolyte interface.[9,16] For H-SOFC, water is generated at the cathode side during operation, which affects the cathode performance more severely for the PCCC than the PBCC, since the water occupies the cathode electrochemical reaction sites and the water vapor partial pressure will be higher for adsorbing more by-product water in the PCCC. Thus, although the PBCC has less TPB or electrochemical reaction sites compared to the PCCC, it will be still able to exhibit a desirable electro-catalytic ability which has been validated by Sun et al.[9]

Recently, La_2NiO_4-based phases with K_2NiF_4-type structure have drawn growing attention as promising candidate materials for the cathode of intermediate temperate SOFCs (IT-SOFCs)[17,18], especially $La_2NiO_{4+\delta}$ (LNO), which has the advantages of exhibiting relatively high oxygen diffusion (D = 2×10^{-7} cm^2 s^{-1}) and surface exchange coefficients (k = 2×10^{-6} cm s^{-1})[19], as well as compatible TEC (~13.0×10^{-6} K^{-1})[20] with solid electrolytes and oxygen over-stoichiometry enabling the transportation of oxygen ions.[17] The crystal structure of LNO can be described as stacked $LaNiO_3$ perovskite layers alternating with La_2O_2 rocksalt layers along the c direction.[21] Significant excess oxygen, denoted as δ, can be incorporated into the La_2O_2 layers to decrease the structural stresses between the La-O and Ni-O bonding. At the same time, electron holes on nickel cations are created to satisfy the electroneutrality conservation while oxygen as interstitial defects in the rocksalt layers.[22] In the LNO-based materials, the interstitial mechanism makes a main contribution to the oxygen ionic transport.[23] In fluorite structure (such as CeO_2), the substitution of Sm^{3+} for Ce^{4+} results in the formation of oxygen vacancies to compensate the charge balance in the lattice. The addition of a small amount of $SmO_{1.5}$ could significantly enhance the ionic conductivity of samples because of the formation of a large number of oxygen vacancies ($V_O^{\bullet\bullet}$) in the fluorite lattice, as expressed by the following reaction.[24]

$$2SmO_{1.5} \xrightarrow{CeO_2} 2Sm'_{Ce} + O_O + V_O^{\bullet\bullet} \qquad (\mathrm{I})$$

And among $(CeO_2)_{1-X}(SmO_{1.5})_X$, $Sm_{0.2}Ce_{0.8}O_{2-\delta}$ has the best ionic conductivity which could arrive at 9.45×10^{-2} S cm^{-1} at 800 °C. Additionally, rhombohedral phase $LaNi_{0.6}Fe_{0.4}O_{3-\delta}$ (LNF) used as SOFC cathode has several advantages, including high electrical

[a]*CAS Key Laboratory of Materials for Energy Conversion & Collaborative Innovation Center of Suzhou Nano Science and Technology, University of Science and Technology of China, Hefei 230026, PR China*
[b]*Physical Sciences and Engineering Division, King Abdullah University of Science and Technology (KAUST), Thuwal 23955-6900, Saudi Arabia*
[c]*Key Laboratory of Materials Physics, Institute of Solid State Physics, Chinese Academy of Sciences, Hefei 230031, PR China*
Email: wliu@ustc.edu.cn (W. Liu) ; lei.bi@kaust.edu.sa
Fax: +86 551 63602586; Tel: +86 551 63606929

conductivity (580 S cm^{-1} at 800 °C)[25], a desirable TEC (average 11.4×10^{-6} K^{-1} from 30 to 1000 °C)[26], high electrochemical activity for the oxygen reduction reaction and excellent durability as regards chromium poisoning.[27]

LNO alone does not show good electronic conductivity (76 S cm^{-1} at 800 °C)[28] which limits its practical application as an SOFC cathode. But it has high oxygen ion conductivity (σ_o) which is ~0.02 S cm^{-1} at 700 °C.[20,23,29-31] Meanwhile, Eguchi et al.[32], Jung et al.[33], Sanghavi et al.[34] and Yahio et al.[35] found out that the σ_o at 973 K reached ~0.02 S cm^{-1} for SDC samples. In general, although the σ_o of SDC and LNO has different values reported in literature, they were in the same order of magnitude in IT ranges (500-700 °C). Considering almost the same σ_o for LNO and SDC, when mixed LNO with LNF and SDC with LNF in the volume ratio of 1:1 to form LNO-LNF and SDC-LNF composite cathodes, the effect of different oxygen transfer mechanism rather than the conductivity values on the cathode performance could be an interesting topic to investigate. So far, there are no reports for the comparison of different oxygen transfer mechanism affecting the cathode performance based on H-SOFCs in the literature. In this work, the chemical compatibility, microstructures and electrochemical performance of LNO-LNF with the interstitial oxygen transfer mechanism and SDC-LNF with the oxygen vacancy transfer mechanism as cathodes were studied in details for the comparison.

2 Experimental

2.1 Preparation of powders

LNO, LNF, SDC and BZCY powders were synthesized via a citric acid-nitrate gel combustion process.[36] The raw materials for synthesis of LNO powders were La_2O_3, $Ni(NO_3)_2$•$6H_2O$ and La_2O_3, $Ni(NO_3)_2$•$6H_2O$ and $Fe(NO_3)_3$•$9H_2O$ were used for synthesize LNF. Sm_2O_3, $Ce(NO_3)_3$•$6H_2O$ and $BaCO_3$, $Zr(NO_3)_4$•$5H_2O$, $Ce(NO_3)_3$•$6H_2O$, $Y(NO_3)_3$•$6H_2O$ served as the raw materials for SDC and BZCY powders respectively. After the combustion, the as-prepared ash-like powders were calcined at 1000, 1000, 600 and 1000 °C for 3 h in air to obtain LNO, LNF, SDC and BZCY powders, respectively.

2.2 Fabrication of symmetric cells and anode-supported single cells

The BZCY substrates for symmetric cells were fabricated with BZCY powders via die-pressing and then sintering at 1500 °C for 5 h in air. The thickness and diameter of the sintered BZCY disks were approximately 1.0 and 12 mm, respectively.

The NiO-BZCY composite powders with a weight ratio of 6:4 for the anode substrates were prepared by the one-step gel combustion process.[36] The composite powders were calcined at 1000 °C for 3 h and then 20 wt.% starch was added as pore-creating materials to form sufficient porosity in the anode. The anode supported half cells were fabricated by a co-pressing method[37] and then co-fired at 1400 °C for 5 h.

LNO and SDC powders were mixed with LNF in the volume ratio 1:1 thoroughly together with a 10 wt.% ethylcellulose-terpineol binder, respectively, to prepare two different cathode slurries (LNO-LNF and SDC-LNF). The slurry was then painted onto the dense BZCY electrolyte disks or membranes and fired at 1000 °C for 3 h in air to form porous cathode layers. Ag paste was applied to the cathode as a current collector and Ag wire was employed as the conducting wire. The effective area of the cathode layer in single cells was 0.237 cm^2.

2.3 Characterization and electrochemical measurements

Phase compositions of the LNO-LNF and SDC-LNF mixed powders fired at 1000 °C were identified by an X-ray diffractometer (Rigaku TTR-Ⅲ) using CuKα radiation. The microstructures of the cell components were investigated by a scanning electron microscopy (SEM, JEOL JSM-6700F).

Symmetric cells for the impedance tests were measured with an impedance analyzer (CHI604B, Shanghai Chenhua) (0.1-100 kHz, 5 mV as AC amplitude) from 550 to 700 °C. The spectrum curve fitting was performed using the ZSimpWin Software. The equivalent circuit used to fit the plots was made of a resistance (R) and an inductance (L) associated in series with two distributed elements, composed by a constant phase element (CPE) in parallel with a resistance.

The two kind single cells were tested in a home-made cell testing system at a temperature range of 550-700 °C under the same conditions for comparison. Humidified hydrogen (~3% H_2O) at a flow rate of 30 ml min^{-1} and ambient air were used as the fuel and the oxidant, respectively. The water vapor pressure about 0.03 atm was achieved by bubbling H_2 through water at about 25 °C. I-V curves of the cells were collected with a DC Electronic Load (ITech Electronics model IT8511) based on a two-probe configuration. The electrochemical impedance spectra were measured under open circuit conditions using an impedance analyzer (CHI604B, Shanghai Chenhua). A 5 mV a.c. signal was applied and the frequency was swept from 100 kHz to 0.1 Hz. Ohmic resistance and polarization resistance of the cells under open circuit conditions were determined from the impedance spectra.

3 Results and discussion

3.1 Chemical stability

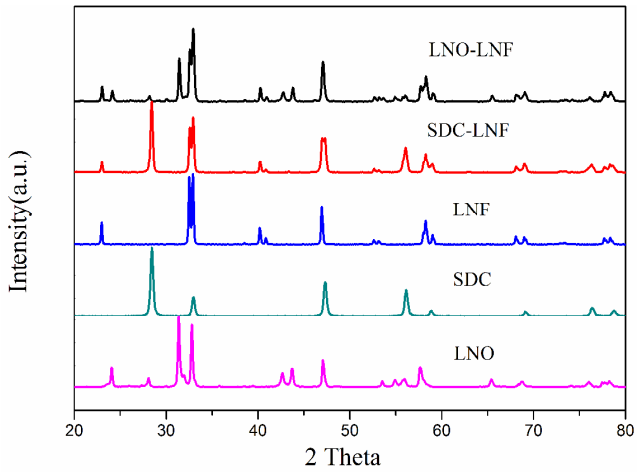

Fig. 1 XRD patterns of dry-mixed powders LNO-LNF and SDC-LNF fired at 1000 °C for 3h.

In order to investigate the chemical compatibility of LNO and SDC with LNF, the phases of LNO-LNF and SDC-LNF mixed powders were studied by the powder XRD technique. Fig. 1 shows

the XRD patterns of two different dry-mixed powders LNO-LNF and SDC-LNF after firing at 1000 °C. In each pattern, only typical peaks corresponding to LNF and LNO or SDC can be found, and no additional peaks corresponding to other secondary phases can be identified. The XRD results suggest that no obvious reactions occurred during the high temperature firing process, implying an excellent chemical compatibility between the rhombohedral phase LNF and the mixed ionic and electronic conductor (MIEC) LNO or the ionic conductor SDC at the temperature up to 1000 °C.

3.2 Characterization of symmetrical cells

Fig. 2(a) shows the typical electrochemical impedance spectra (EIS) in Nyquist plot for LNO-LNF|BZCY|LNO-LNF and SDC-LNF|BZCY|SDC-LNF symmetrical cells at 700 °C. It can be seen from Fig. 2(a), the spectra measured with different cathodes show overlapped semi-circles, implying more than one electrode process. The impedance spectra were fitted according to an $LR(R_HQ_H)(R_LQ_L)$ equivalent circuit model. The (RQ) components correspond to the involved electrode processes. For (RQ) components, R is the resistance and Q is the constant phase element. The impedance Z_Q of a constant phase element Q and equivalent capacitance C of the (RQ) components can be calculated according to the following equations[38]:

$$Z_Q = \frac{1}{Q(i\cdot\omega)^n} \quad (1)$$

$$C = \frac{(RQ)^{1/n}}{R} \quad (2)$$

where, ω is the angular frequency and n is an exponent. The constant phase element Q represents an ideal capacitor and an ideal resistor when n=1 and n=0, respectively. When 0<n<1, the circuit component reflects inhomogeneity of the electrode system. The relaxation frequency of an electrode process corresponding to a specific (RQ) component can be calculated by the following equation[38]:

$$f = \frac{(RQ)^{-1/n}}{2\pi} \quad (3)$$

Table 1 lists the parameters of the circuit elements which are derived from Fig. 2(a). The electrode process corresponding to the component (R_HQ_H) had the equivalent capacitances of 10^{-5}-10^{-4} F cm^{-2} and the relaxation frequencies of 10^3-10^4 Hz with different cathodes. Thus, the electrode process is normally attributed to the charge transfer process of oxygen ions between the electrode and electrolyte[17,39]. The electrode processes corresponding to the component (R_LQ_L) which shows the equivalent capacitances of 10^{-4}-10^{-2} F cm^{-2} along with the relaxation frequencies of 10^0-10^2 Hz. Accordingly, the former process is generally regarded as the diffusion of atomic oxygen within the porous electrode followed by a charge transfer (surface oxygen exchange), while the latter can be ascribed to the adsorption and dissociation of molecular oxygen on the surface of the electrode[17,40]. The typical EIS in Nyquist plots at 550-650 °C showing a similar shape is not shown here.

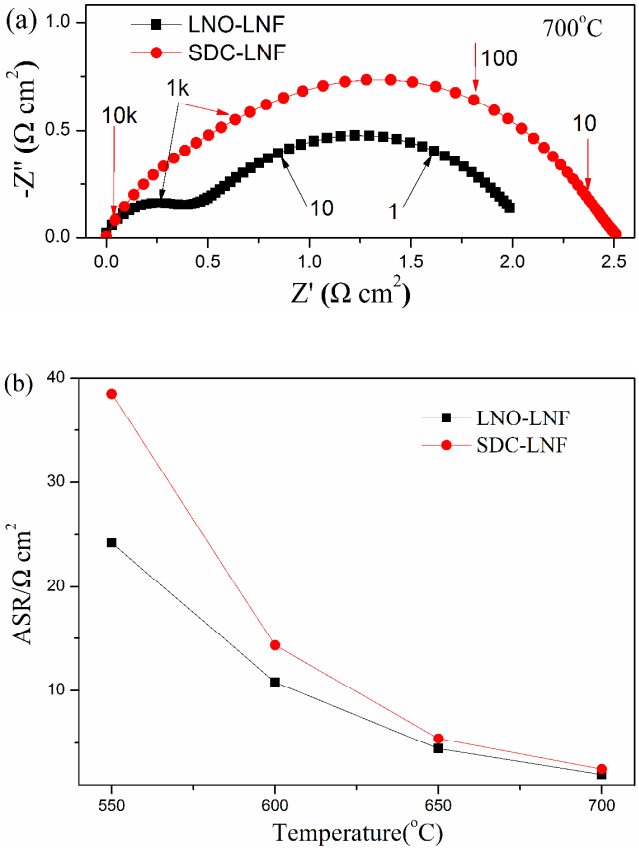

Fig. 2 (a) EIS of symmetric cells with LNO-LNF and SDC-LNF cathode at 700 °C, and (b) the ASR comparison of two different cathodes from 550 to 700 °C.

The area specific resistances (ASRs) of two kind electrodes in temperature range of 550-700 °C are shown in Fig. 2(b). An obvious drop of the ASR value can be observed for two cells with the increasing temperature. In addition, LNO-LNF displays lower of ASR values at the same temperature than that of SDC-LNF which will be interpreted at the later discussion.

To know the cathode process, the understanding of cathode elementary steps for H-SOFCs is very important. He et al.[41] have subdivided the elementary steps for the H-SOFC cathode reaction based on characteristics of protons' transfer and reaction. Fig. 3 is a schematic diagram of the oxygen reduction reaction (ORR) at LNO-LNF and SDC-LNF cathode based on BZCY electrolyte. The overall ORR at the cathode and incorporation into the ionic conductor is described in Krögere-Vink notation as:

$$O_2 + 4e^- \rightarrow 2O''_{O,LNO} \quad \text{(for LNO-LNF cathode)} \quad (\text{II})$$

$$O_2 + 4e^- + 2V_O^{\bullet\bullet} \rightarrow 2O^{\times}_{O,SDC} \quad \text{(for SDC-LNF cathode)} \quad (\text{III})$$

It is generally accepted that the oxygen reduction at the cathode could be described with the most plausible rate-limiting steps as follows[41]:

Table 1 Results of the electrochemical impedance spectra for LNO-LNF and SDC-LNF cathode at 700 °C.

Electrode composition	R_H (Ω cm^2)	C_H (F cm^2)	f_H (Hz)	R_L (Ω cm^2)	C_L (F cm^2)	f_L (Hz)
LNO-LNF	0.419	1.2×10^{-4}	3164	1.568	3.89×10^{-2}	2.61
SDC-LNF	0.635	3.04×10^{-5}	8252	1.872	3.29×10^{-4}	258.8

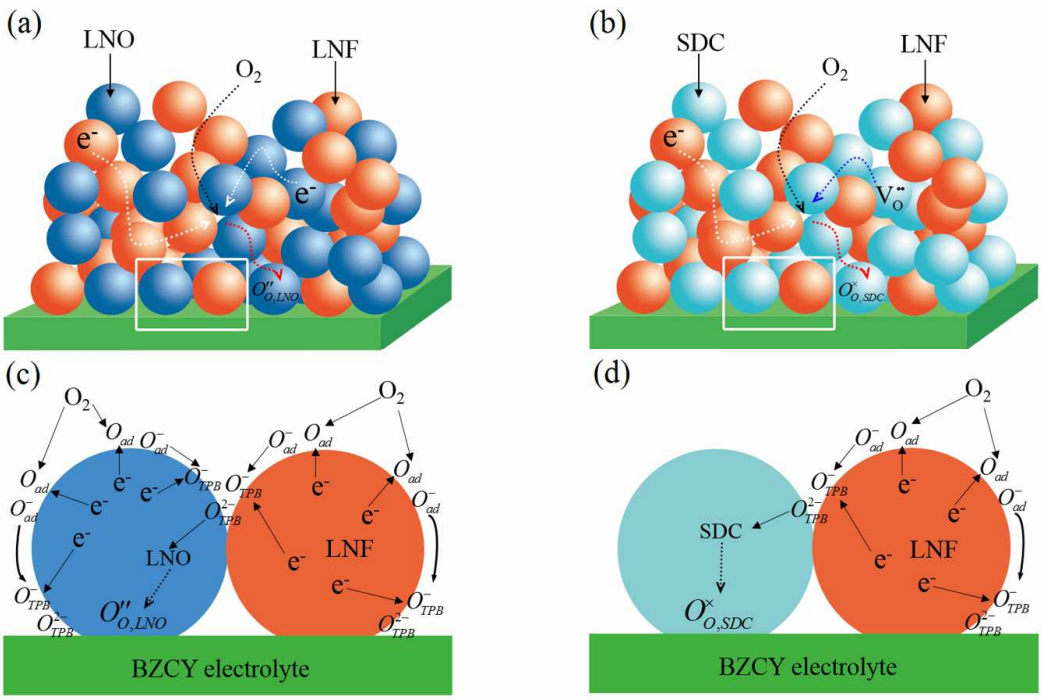

Fig. 3 Schematic diagrams of overall ORR at (a) LNO-LNF cathode and (b) SDC-LNF cathode with BZCY electrolyte, and an ORR model at the cathode (c) LNO-LNF/electrolyte (BZCY) interface and (d) SDC-LNF/electrolyte (BZCY) interface.

Table 2 R_H and R_L values of the electrochemical impedance spectra for LNO-LNF and SDC-LNF at 550-700 °C. The electrolyte resistance was subtracted from the cell impedance and only polarization resistance (Rp) was shown here.

R_H and R_L (Ω cm^2)	LNO-LNF		SDC-LNF	
	R_H	R_L	R_H	R_L
700 °C	0.419	1.568	0.635	1.872
650 °C	0.975	3.488	1.077	4.347
600 °C	2.438	8.341	3.06	11.28
550 °C	5.3	18.93	7.8	30.7

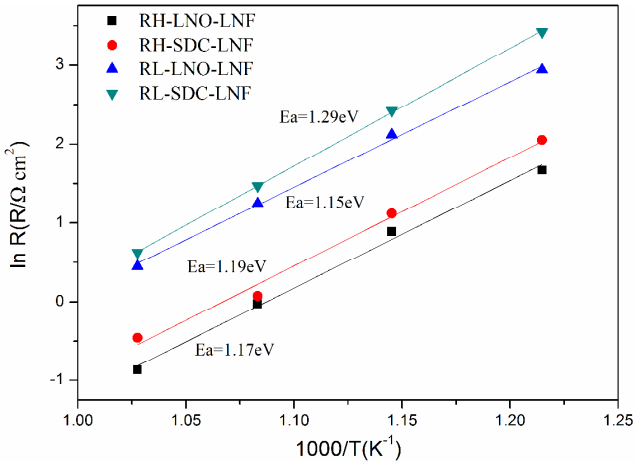

Fig. 4 Arrhenius plots for resistance of LNO-LNF and SDC-LNF cathode on BZCY electrolyte at high frequency (R_H) and low frequency (R_L).

Step 1 $O_2 \rightarrow 2O_{ad}$ (dissociative adsorption)

Step 2 $O_{ad} + e^- \rightarrow O_{ad}^-$ (charge transfer)

Step 3 $O_{ad}^- \rightarrow O_{TPB}^-$ (surface diffusion)

Step 4 $O_{TPB}^- + e^- \rightarrow O_{TPB}^{2-}$ (charge transfer at TPB)

For LNO-LNF, the O_{TPB}^{2-} at the TPB of LNF-LNO-gas could be immediately incorporated in interstitial sites of LNO which can be described as step 5.

Step 5 $O_{TPB}^{2-} \rightarrow O''_{O,LNO}$

However, for SDC-LNF, there are many vacancies ($V_O^{\bullet\bullet}$) existed. The O_{TPB}^{2-} at the TPB of LNF-SDC-gas could be incorporated into the SDC combining with the oxygen vacancies, the elementary step is as step 6.

Step 6 $O_{TPB}^{2-} + V_{O,SDC}^{\bullet\bullet} \rightarrow O_{O,SDC}^{\times}$

The R_H and R_L values of the two symmetrical cells at 550-700 °C are listed in Table 2. From which we can see that the polarization resistances of various electrode processes (R_H and R_L) presented an identical variation trend, both increase with decreasing of the temperature. However, both R_H and R_L of SDC-LNF are larger than that of LNO-LNF. The plausible reason for this phenomenon is the more easy generation and transportation of oxygen ions in LNO-LNF compared with that in SDC-LNF. It is clear that the incorporation reaction at the electrode and electrolyte is not the rate limiting step ($R_H < R_L$ in both cathodes). Fig. 4 shows the Arrhenius plots for resistance of LNO-LNF and SDC-LNF cathode on BZCY electrolyte at high frequency (R_H) and low frequency (R_L). The activation energy (Ea) of R_H with LNO-LNF and SDC-LNF are 1.17 and 1.19 eV, while the Ea of R_L are 1.15 and 1.29 eV, respectively. We can see that the Ea of R_H with the cathode LNO-LNF was a little lower, which could ascribe to extra LNO-BZCY-gas TPBs in the LNO-LNF cathode and

BZCY electrolyte interface compared with SDC-LNF cathode as shown in Fig. 3(c). The extra LNO-BZCY-gas TPBs will result in more electrochemical reaction sites for the incorporation reaction at the electrode and electrolyte which may have contribution to the lower Ea of R_H with LNO-LNF. However, the Ea of R_L with SDC-LNF are much higher than that of LNO-LNF, which might be attributed to the higher binding energy of O_{TPB}^{2-} with $V_{O,SDC}^{\bullet\bullet}$ to form the $O_{O,SDC}^{\times}$ shown in step 6. At the same time, the O_{TPB}^{2-} immediately incorporates at interstitial sites of LNO with a relatively low binding energy which can promote LNO having easier oxygen surface exchange. Furthermore, LNO-LNF has more ORR paths than SDC-LNF as shown in Fig. 3(c).

Evidently, the oxygen transfer from the cathode surface to the electrolyte surface is not the rate-limiting process for the similar ionic conductivity and oxygen self-diffusion coefficient (2×10^{-7} cm^2 s^{-1})[19] of SDC and LNO. It is also evidenced by the smaller difference in the resistance of high frequency region and the Ea of R_H. Therefore, the lower ASR of LNO-LNF is mainly dominated by the low frequency process, which is attributed to the superiority of LNO in the surface oxygen exchange process that is reflected by the lower Ea of R_L. Moreover, the surface oxygen exchange is closely related to the oxygen transfer mechanism (as stated in equation Ⅱ and Ⅲ).

3.3 Electrochemical Performance of single cells

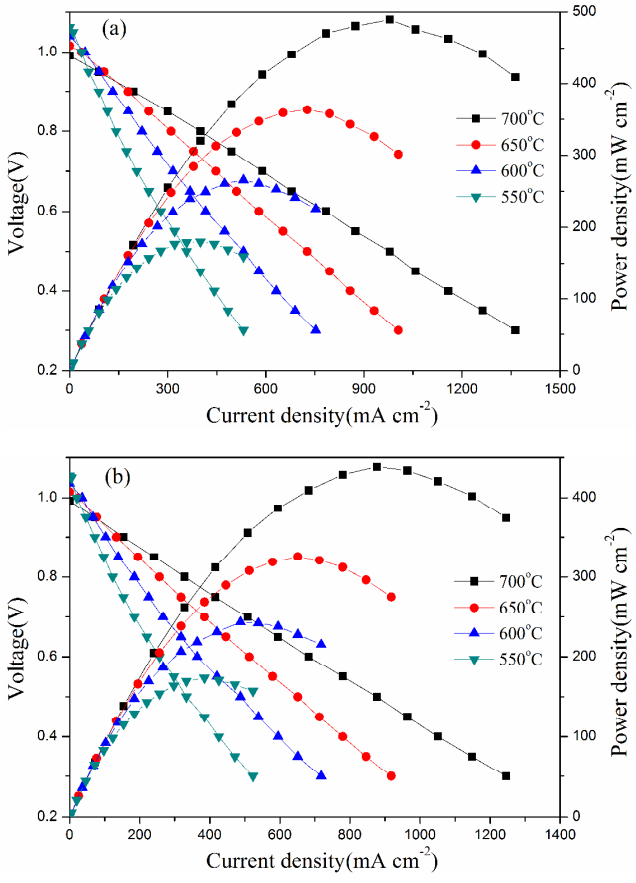

Fig. 5 I-V and I-P curves of the single cell with the cathode (a) LNO-LNF and (b) SDC-LNF at 550-700 °C.

To characterize the cathode performance of LNO-LNF and SDC-LNF composite cathodes, different button cells using NiO-BZCY as the anode and BZCY as the electrolyte were fabricated and measured under conventional conditions (humidified hydrogen as the fuel gas; static air as the oxidant). As the different single cells were fabricated in the same synthesis method, and have almost the identical thick BZCY electrolyte, it can be considered that the discrepancy in electrochemical efficiency was caused by the different cathode used. Fig. 5(a) and Fig. 5(b) show the typical I-V and I-P curves of single cells with two different cathodes at 550-700 °C. The open-circuit voltages (OCVs) of the single cell with LNO-LNF cathode after anode reduction are 0.991, 1.016, 1.041 and 1.062V, and the maximum power densities (MPDs) are 490, 364, 266 and 180 mW cm^{-2} at 700, 650, 600 and 550 °C, respectively. In contrast, the cell NiO-BZCY|BZCY|SDC-LNF outputs the OCVs of 0.992, 1.015, 1.036 and 1.055V, corresponding to the MPDs that are 439, 326, 244 and 173 mW cm^{-2} at 700, 650, 600 and 550 °C, respectively. We can see that both the OCV values of the single cells with LNO-LNF and SDC-LNF as cathode confirm that the electrolyte membranes in different single cells are sufficiently dense to prevent any gas leakage. At all testing temperatures, the single cell with LNO-LNF cathode shows higher MPDs than that with SDC-LNF cathode, which suggests that LNO-LNF cathode has better electrochemical properties.

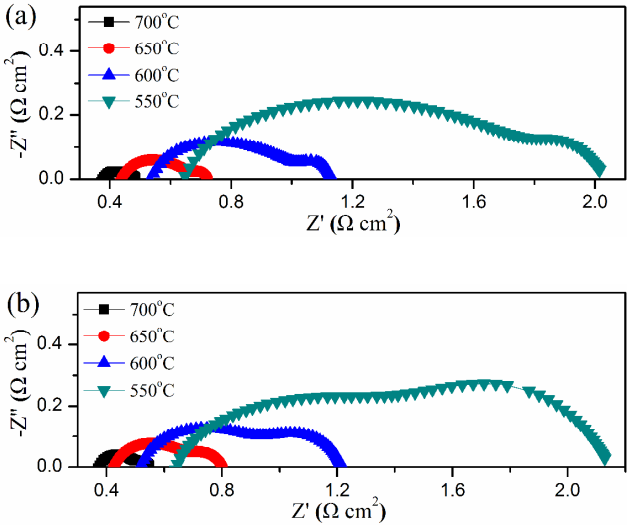

Fig. 6 EIS of the single cell with (a) LNO-LNF and (b) SDC-LNF cathode measured under open-circuit conditions from 550 to 700 °C.

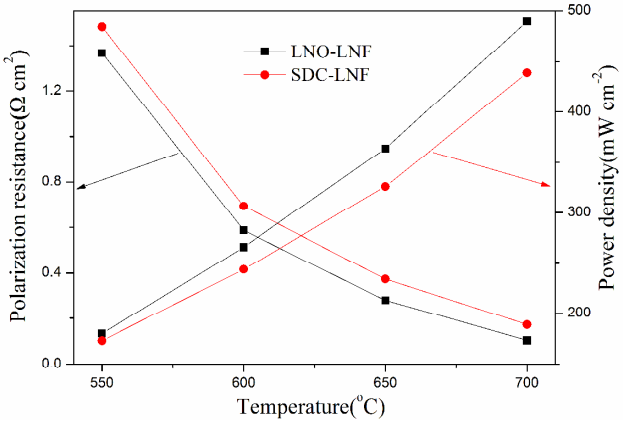

Fig. 7 The MPDs and the R_p of two different single cells at 550-700 °C.

Table 3 R_o and R_p of single cells with LNO-LNF and SDC-LNF as cathode measured from 550 to 700 °C.

R_o and R_p (Ω cm^2)	550 °C		600 °C		650 °C		700 °C	
	R_o	R_p	R_o	R_p	R_o	R_p	R_o	R_p
LNO-LNF	0.648	1.367	0.543	0.587	0.442	0.279	0.381	0.103
SDC-LNF	0.647	1.482	0.521	0.693	0.426	0.374	0.376	0.172

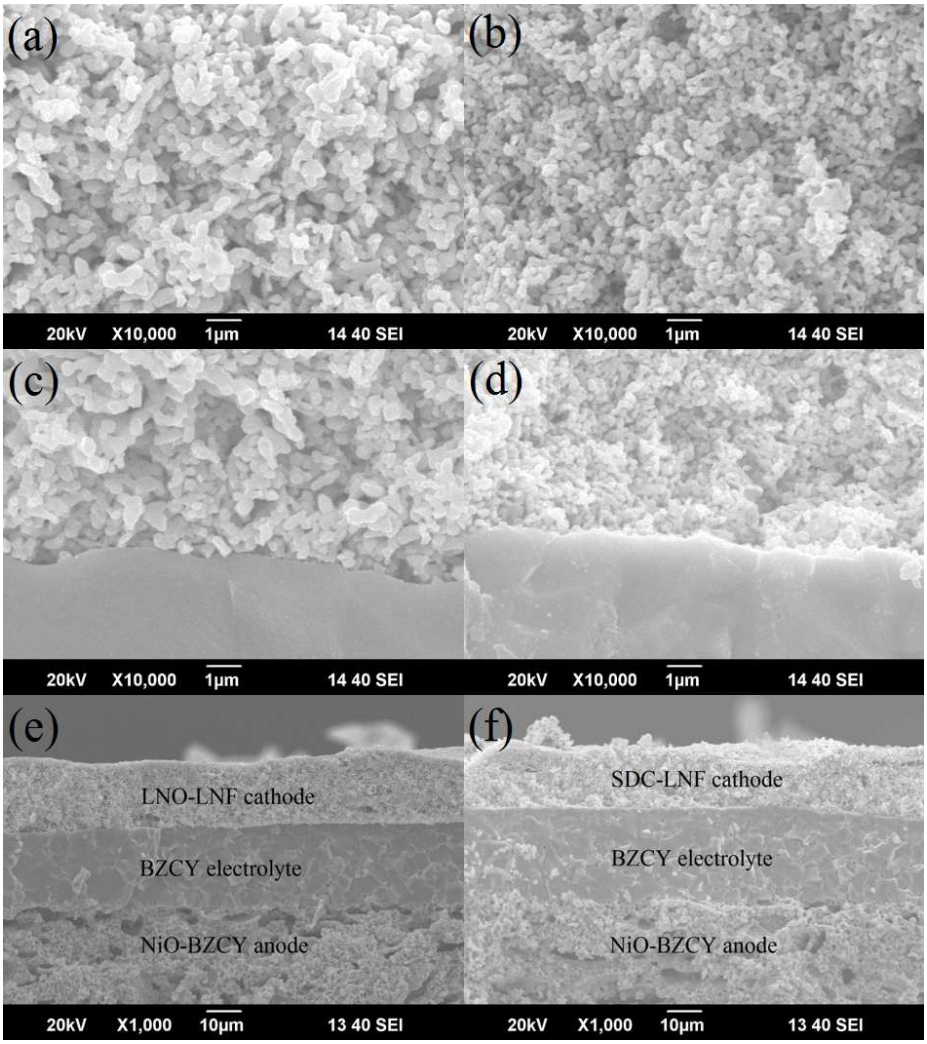

Fig. 8 Cross-section SEM images of (a) LNO-LNF and (b) SDC-LNF cathode layer, the interfaces between the (c) LNO-LNF or (d) SDC-LNF cathode layer and the BZCY electrolyte membranes, and the single cell with the cathode (e) LNO-LNF and (f) SDC-LNF after testing.

Typical EIS at 550-700 °C with the cathode LNO-LNF and SDC-LNF were obtained under open-circuit conditions to provide an insight understanding of how each cathode works at the fuel cell conditions, as shown in Fig. 6(a) and Fig. 6(b). In the EIS plots, the high-frequency intercept corresponds to the ohmic resistance (R_o) of the cell, including the ionic resistance of the electrolyte, the electronic resistance of the electrodes and some contact resistance associated with the interfaces of the components. The low frequency intercept corresponds to the total resistance (R_t) of the cell. The difference between the two intercept indicates the interfacial polarization resistance (R_p) of the cell. The R_o and R_p of the two different single cells range of 550-700 °C are shown in Table 3. As can be seen from Table 3, all resistances decrease with increasing temperature, making it clear that the corresponding electrochemical reactions are thermally activated processes. The R_p values of the cell with SDC-LNF cathode decrease from 1.482 to 0.172 Ω cm^2 with increasing temperature from 550 to 700 °C. Nevertheless, the R_o only decreases from 0.647 to 0.376 Ω cm^2 under the same conditions. Noticeably, the cell R_p governs the downward trend of R_t and plays a major role in determining the total resistance of the cell below 600 °C. Then the purpose of developing high-performance cathode materials is to reduce R_p and thus to enhance the cell performance, which ultimately realizes low-temperature cell operations. Evidently, LNO-LNF has lower Rp values of 0.103, 0.279, 0.587 and 1.367 Ω cm^2 at 700, 650, 600 and 550 °C, respectively, which is consistent with higher power output discussed before.

To further analyze the electrochemical parameters, the MPDs and the R_p of single cells with two different cathodes are shown in Fig. 7. It is clear that the single cell with LNO-LNF or SDC-LNF as cathode generates the gradually increased power output with increasing the test temperature. Meanwhile, the Rp indicates the

contrary trends. The single cell NiO-BZCY|BZCY|LNO-LNF shows higher power output and lower R_p in the test temperature range. Notably, the power performance is higher than most of the previously reported similar single cells with cobalt-free cathodes, including $La_{0.7}Sr_{0.3}FeO_{3-\delta}$-SDC (449 mW cm^{-2} at 700 °C)[9], $BaCe_{0.5}Bi_{0.5}O_{3-\delta}$ (321 mW cm^{-2} at 700 °C)[15], $BaCe_{0.5}Fe_{0.5}O_{3-\delta}$ (395 mW cm^{-2} at 700 °C)[42], $GaBaFeNiO_{5+\delta}$ (456 mW cm^{-2} at 700 °C)[43] and $La_{0.6}Sr_{0.4}Fe_{0.9}Ni_{0.1}O_{3-\delta}$ (405 mW cm^{-2} at 700 °C)[44]. For the densities of LNO and LNF have small disparity, the 1:1 volume ratio LNO-LNF cathode is very close to LNO-LNF55 cathode reported by Hou et al.[1] However, the MPDs in this work are a little lower, which may be attributed to the thicker BZCY electrolyte used in this study which is about 24 μm.

The microstructures of the cells were observed by SEM. Fig. 8 shows cross-sectional views of LNO-LNF and SDC-LNF cathode layers, the interfaces between the LNO-LNF or SDC-LNF cathode layer and the BZCY electrolyte membrane, and single cells with two different cathodes after testing. Fig. 8(a) and Fig. 8(b) show the cross-section morphologies of the LNO-LNF and SDC-LNF cathode layers, respectively. It can be clearly observed that both two cathode layers have a uniform and porous structure, with the particles interconnecting well with each other. The particles in two cathodes are almost in nanoscale with continuous pores, which significantly favors gas diffusion and electrochemical reactions in the cathode. Fig. 8(c) and Fig. 8(d) show the morphologies of the interfaces between the electrolyte membrane and two different cathode layers of the tested cells. Though the cells have suffered a heating and subsequent cooling process during testing, the cathode layers still bond to the electrolyte membranes tightly. The close adhesion confirms that both the LNO-LNF and SDC-LNF composite cathodes show good thermal matching with the BZCY electrolyte, which is also an important consideration in the design of a composite cathode. As shown in Fig. 8(e) and Fig. 8(f), in both two single cells, both anode and cathode well adhered on both side of dense BZCY electrolyte without any sign of cracking or delamination. The cathode microstructures for both cells are quite similar with the same electrolyte thickness of 24 μm. Therefore, the different single cell performance should be owning to the intrinsic properties of different cathode materials.

3.4 Optimization of the single cell with LNO-LNF cathode

The NiO-BZCY composite powders with a weight ratio of 65:35 was applied as the anode substrates while the one with the weight ratio of 6:4 as anode functional layer (AFL). The optimized single cell with LNO-LNF cathode has four-layer containing the anode, AFL (~12 μm), electrolyte (~14 μm) and cathode which was shown in Fig. 9. It can be seen that the BZCY electrolyte film is fully dense, free from crack and bonds firmly to the electrode layers. The good microstructure is beneficial for obtaining single cells with high power performance as the reduced electrolyte can effectively reduce the ohmic resistance of the total cell and the AFL can provide more active sites for electrochemical reactions. The OCVs of the optimized single cell were 0.99, 1.01, 1.037 V at 700, 650 and 600 °C respectively, further confirming the high density of the electrolyte film. The I-V and I-P curves of the optimized single cell is presented in Fig. 10. One can see that the cell exhibits an excellent power performance. The MPDs achieved 708, 542 and 352 mW cm^{-2} at 700, 650 and 600 °C, respectively. The cell performance is largely improved compared to the un-optimized single cell with the same cathode. In addition, this cell performance is also one of the largest MPDs ever reported.

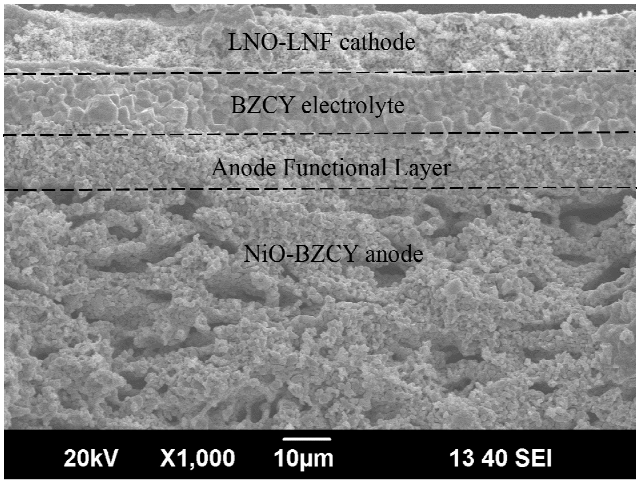

Fig. 9 SEM image of cross-sectional morphology of the optimized single cell with LNO-LNF cathode.

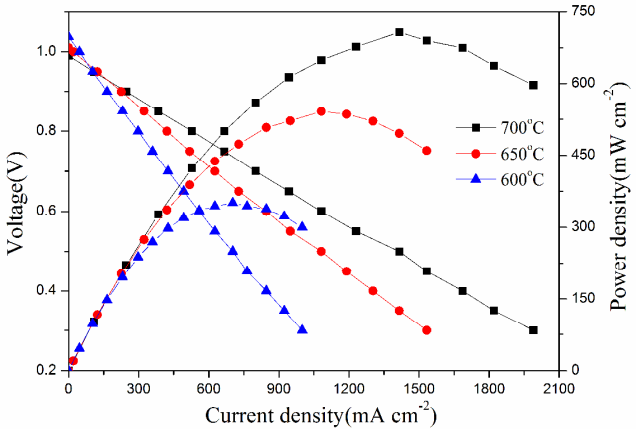

Fig. 10 I-V and I-P curves of the optimized single cell with LNO-LNF cathode.

4. Conclusions

The performance of LNO-LNF with the interstitial oxygen transfer mechanism and SDC-LNF with the oxygen vacancy transfer mechanism as cathodes for BZCY-based H-SOFCs were studied in detail. The excellent chemical compatibility between the MIEC LNO or the ionic conductor SDC and the rhombohedral phase LNF at 1000 °C has been ascertained using XRD. In symmetrical cells, LNO-LNF cathode showed lower area specific polarization resistances than that for SDC-LNF under the same testing conditions. The electrochemical performances of both composite cathodes were investigated comparatively, including OCVs, polarization resistances, and maximum power densities in single cells. Obviously, the cell with LNO-LNF cathode produced lower polarization resistances and higher maximum power densities than that with SDC-LNF cathode. These results indicate it that LNO-LNF cathode is superior to SDC-LNF cathode for H-SOFCs. The power outputs of the optimized single cell NiO-BZCY|AFL|BZCY|LNO-LNF with an AFL reached an encouraging performance of 708 mW cm^{-2} at 700°C. Compared with the oxygen

vacancy transfer mechanism in SDC-LNF, the interstitial oxygen transfer mechanism in LNO-LNF is a more preferable alternative as proton-blocking composite cathode in the design of the cathode materials for H-SOFCs. The applications of a material with a higher oxygen surface exchange coefficient might be another promising route for further improving the cathode performance as both SDC and LNO have only moderate oxygen surface exchange coefficient values and this aspect is worth studying in the future.

Acknowledgements

This work was supported by Ministry of Science and Technology of China (Grant No: 2012CB215403). The project was also supported by the National Science Foundations of China (Grant Nos: 51472228 and 21406190).

References

1 J. Hou, Z. Zhu, J. Qian and W. Liu, *J. Power Sources*, 2014, 264, 67-75.
2 L. Bi, S. Boulfrad and E. Traversa, *Chem. Soc. Rev.*, 2014, 43, 8255-8270.
3 Z. Wang, M. Liu, W. Sun, D. Ding, Z. Lü and M. Liu, *Electrochem. Commun.*, 2013, 27, 19-21.
4 L. Bi and E. Traversa, *J. Mater. Res.*, 2013, 29, 1-15.
5 E. Fabbri, I. Markus, L. Bi, D. Pergolesi and E. Traversa, *Solid State Ionics*, 2011, 202, 30-35.6.
6 F. Zhao, Q. Liu, S. Wang, K. Brinkman and F. Chen, *Int. J. Hydrogen Energy*, 2010, 35, 4258-4263.
7 X.-Z. Fu, J.-L. Luo, A. R. Sanger, N. Luo and K. T. Chuang, *J. Power Sources*, 2010, 195, 2659-2663.
8 E. Fabbri, A. Depifanio, E. Dibartolomeo, S. Licoccia and E. Traversa, *Solid State Ionics*, 2008, 179, 558-564.
9 W. Sun, S. Fang, L. Yan and W. Liu, *J. Electrochem. Soc.*, 2011, 158, B1432.
10 L. Bi, S. Zhang, S. Fang, Z. Tao, R. Peng and W. Liu, *Electrochem. Commun.*, 2008, 10, 1598-1601.
11 C. Zuo, S. Zha, M. Liu, M. Hatano and M. Uchiyama, *Adv. Mater.*, 2006, 18, 3318-3320.
12 Z. Zhu, J. Qian, Z. Wang, J. Dang and W. Liu, *J. Alloys Compd.*, 2013, 581, 832-835.
13 H. Ding, B. Lin, X. Liu and G. Meng, *Electrochem. Commun.*, 2008, 10, 1388-1391.
14 W. Sun, Z. Shi, S. Fang, L. Yan, Z. Zhu and W. Liu, *Int. J. Hydrogen Energy*, 2010, 35, 7925-7929.
15 Z. Tao, L. Bi, L. Yan, W. Sun, Z. Zhu, R. Peng and W. Liu, *Electrochem. Commun.*, 2009, 11, 688-690.
16 R. Peng, T. Wu, W. Liu, X. Liu and G. Meng, *J. Mater. Chem.*, 2010, 20, 6218.
17 K. Zhao, Q. Xu, D.-P. Huang, M. Chen and B.-H. Kim, *J. Solid State Electrochem.*, 2012, 16, 2797-2804.
18 R. Sayers, J. E. Parker, C. C. Tang and S. J. Skinner, *J. Mater. Chem.*, 2012, 22, 3536.
19 C. Laberty, F. Zhao, K. E. Swider-Lyons and A. V. Virkar, *Electrochem. Solid State Lett.*, 2007, 10, B170.
20 V. V. Kharton, A. P. Viskup, E. N. Naumovich and F. M. B. Marques, *J. Mater. Chem.*, 1999, 9, 2623-2629.
21 Y. Shen, H. Zhao, K. Świerczek, Z. Du and Z. Xie, *J. Power Sources*, 2013, 240, 759-765.
22 J. Rodriguezcarvajal, M. T. Fernandezdiaz and J. L. Martinez, *J. Phys. Condens. Matter.*, 1991, 3, 3215-3234.
23 Y. Shen, H. Zhao, X. Liu and N. Xu, *Phys. Chem. Chem. Phys.*, 2010, 12, 15124-15131.
24 H. Yahiro, Y. Eguchi, K. Eguchi and H. Arai, *J. Appl. Electrochem.*, 1988, 18, 527-531.
25 S. P. Simner, J. F. Bonnett, N. L. Canfield, K. D. Meinhardt, V. L. Sprenkle and J. W. Stevenson, *Electrochem. Solid State Lett.*, 2002, 5, A173.
26 R. Chiba, F. Yoshimura and Y. Sakurai, *Solid State Ionics*, 1999, 124, 281-288.
27 B. Huang, X.-j. Zhu, Y. Lv and H. Liu, *J. Power Sources*, 2012, 209, 209-219.
28 D.-P. Huang, Q. Xu, W. Chen, F. Zhang and H.-X. Liu, *Ceram. Int.*, 2008, 34, 651-655.
29 A. L. Shaula, E. N. Naumovich, A. P. Viskup, V. V. Pankov, A. V. Kovalevsky and V. V. Kharton, *Solid State Ionics*, 2009, 180, 812-816.
30 H. Zhao, F. Mauvy, C. Lalanne, J. Bassat, S. Fourcade and J. Grenier, *Solid State Ionics*, 2008, 179, 2000-2005.
31 J. Bassat, *Solid State Ionics*, 2004, 167, 341-347.
32 T. S. K. Eguchi, T. Inoue, H. Arai, *Solid State Ionics*, 1992, 52, 165-172.
33 K. E. Hidenori Yahiro, Hiromichi Arai, *Solid State Ionics*, 1989, 36, 71-75.
34 R. Sanghavi, R. Devanathan, M. I. Nandasiri, S. Kuchibhatla, L. Kovarik, S. Thevuthasan and S. Prasad, *Solid State Ionics*, 2011, 204, 13-19.
35 T.-J. H. Guor-Bin Jung, Chung-Liang Chang, *J. Solid State Electrochem.*, 2002, 6, 225-230.
36 W. Sun, L. Yan, B. Lin, S. Zhang and W. Liu, *J. Power Sources*, 2010, 195, 3155-3158.
37 W. Sun, L. Yan, Z. Shi, Z. Zhu and W. Liu, *J. Power Sources*, 2010, 195, 4727-4730.
38 D. Chen, R. Ran, K. Zhang, J. Wang and Z. Shao, *J. Power Sources*, 2009, 188, 96-105.
39 M. J. Escudero, A. Aguadero, J. A. Alonso and L. Daza, *J. Electroanal. Chem.*, 2007, 611, 107-116.
40 K. Zhao, Q. Xu, D.-P. Huang, M. Chen and B.-H. Kim, *Ionics*, 2011, 18, 75-83.
41 F. He, T. Wu, R. Peng and C. Xia, *J. Power Sources*, 2009, 194, 263-268.
42 Z. Tao, L. Bi, Z. Zhu and W. Liu, *J. Power Sources*, 2009, 194, 801-804.
43 Z. Yang, Z. Ding, J. Xiao, H. Zhang, G. Ma and Z. Zhou, *J. Power Sources*, 2012, 220, 15-19.
44 F. Zhang, Z. Yang, H. Wang, W. Wang and G. Ma, *Fuel Cells*, 2012, 12, 749-753.

PAPER www.rsc.org/materials | Journal of Materials Chemistry A

The effect of oxygen transfer mechanism on the cathode performance based on proton-conducting solid oxide fuel cells

Jie Hou[a], Jing Qian[a], Lei Bi[b,*], Zheng Gong[a], Ranran Peng[a] and Wei Liu[a,c,*]

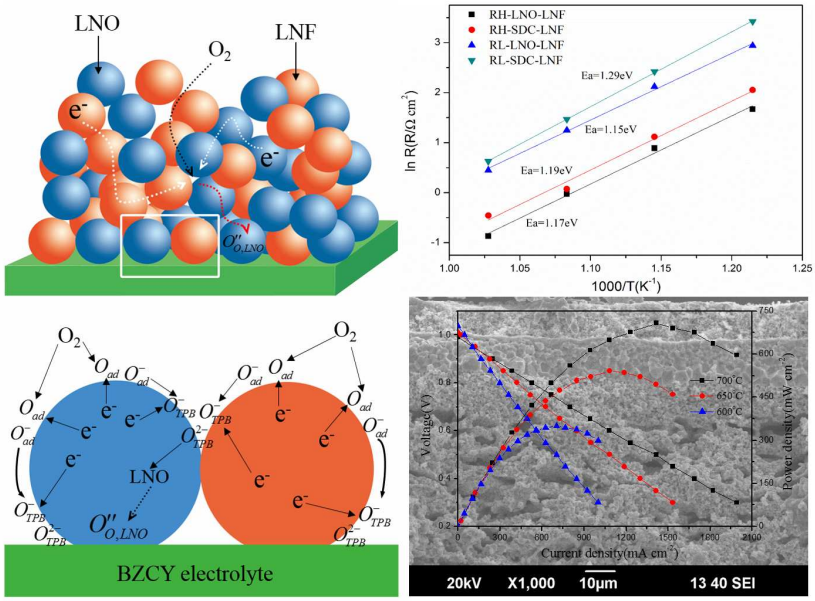

Two different kind proton-blocking composite cathode materials with different oxygen transfer mechanism used for H-SOFCs were firstly evaluated.